ACS APPLIED MATERIALS & INTERFACES

Research Article

www.acsami.org

Construction of 3D Micropatterned Surfaces with Wormlike and Superhydrophilic PEG Brushes To Detect Dysfunctional Cells

Jianwen Hou,[†,‡] Qiang Shi,*[,†] Wei Ye,[†,‡] Qunfu Fan,[§] Hengchong Shi,[†] Shing-Chung Wong,[⊥] Xiaodong Xu,[§] and Jinghua Yin*[,†]

[†]State Key Laboratory of Polymer Physics and Chemistry, Changchun Institute of Applied Chemistry, Chinese Academy of Sciences, Changchun 130022, P. R. China

[‡]University of Chinese Academy of Sciences, Beijing 100049, P. R. China

[§]Polymer Materials Research Center, College of Materials Science and Chemical Engineering, Harbin Engineering University, Harbin 150001, P. R. China

[⊥]Department of Mechanical Engineering, University of Akron, Akron, Ohio 44325-3903, United States

Supporting Information

ABSTRACT: Detection of dysfunctional and apoptotic cells plays an important role in clinical diagnosis and therapy. To develop a portable and user-friendly platform for dysfunctional and aging cell detection, we present a facile method to construct 3D patterns on the surface of styrene-*b*-(ethylene-*co*-butylene)-*b*-styrene elastomer (SEBS) with poly(ethylene glycol) brushes. Normal red blood cells (RBCs) and lysed RBCs (dysfunctional cells) are used as model cells. The strategy is based on the fact that poly(ethylene glycol) brushes tend to interact with phosphatidylserine, which is in the inner leaflet of normal cell membranes but becomes exposed in abnormal or apoptotic cell membranes. We demonstrate that varied patterned surfaces can be obtained by selectively patterning atom transfer radical polymerization (ATRP) initiators on the SEBS surface via an aqueous-based method and growing PEG brushes through surface-initiated atom transfer radical polymerization. The relatively high initiator density and polymerization temperature facilitate formation of PEG brushes in high density, which gives brushes worm-like morphology and superhydrophilic property; the tendency of dysfunctional cells adhered on the patterned surfaces is completely different from well-defined arrays of normal cells on the patterned surfaces, providing a facile method to detect dysfunctional cells effectively. The PEG-patterned surfaces are also applicable to detect apoptotic HeLa cells. The simplicity and easy handling of the described technique shows the potential application in microdiagnostic devices.

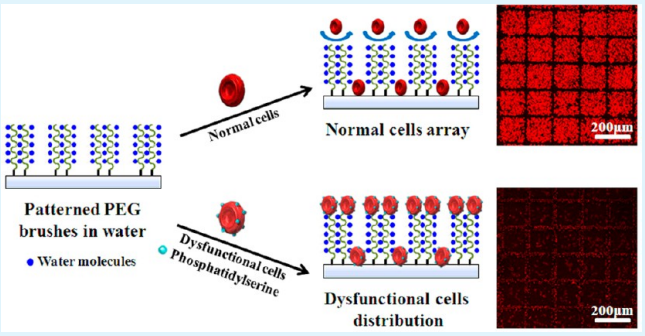

KEYWORDS: *superhydrophilicity, 3D patterned surface, poly(ethylene glycol) brushes, phosphatidylserine, dysfunctional cell detection*

1. INTRODUCTION

Detection of dysfunctional and apoptotic cells in biological fluids plays an important role in clinical diagnosis and therapy.[1−3] Many ex vivo methods based on micromechanical oscillators, microfluidic devices, capillary electrophoresis, and biosensors have been developed.[3−5] However, these methods often need special techniques, equipment, or a skilled person to interpret the results.[3] Furthermore, because most detection methods enumerate abnormal cells in a small volume (5−20 mL) of blood drawn from patients and the rarity of abnormal cells in biological fluids, these methods often fail in detecting exceedingly rare populations.[6−8] In addition, the potential damage to detected cells constrains the collection of abnormal cells for later analysis to investigate their role in disease progression.[9−11] Hence, development of facile and user-friendly detection platforms capable of interrogating the high efficiency and are harmless to detected cells is necessary to realize the enormous diagnostic potential of pathogenic and dysfunctional cells.

Surface patterning provides a powerful tool to create and model cues on soft materials, which define the cell's microenvironment in spatially confined areas and control cell adhesion and spreading.[12−21] Among them, 3D patterning the surface with polymer brushes is emerging as a powerful platform to engineer a surface by providing abundant spatially distributed chemical and physical properties.[22−28] In addition, densely packed polymer brushes with good control of molecular weights and macromolecular architectures can be created by surface-initiated atom transfer radical polymerization (SI-ATRP).[29−36] However, precise construction of a 3D

Received: August 8, 2014
Accepted: November 6, 2014
Published: November 6, 2014

patterned surface to effectively detect dysfunctional cells remains a challenge.

The key strategy for detection of dysfunctional cells on patterned surfaces is that polymer brushes should have an ability to interact oppositely with normal and dysfunctional cells. In this sense, poly(ethylene glycol) (PEG) brushes are good candidates for patterning the surface to effectively detect dysfunctional cells in a harmless manner. On one hand, PEG brushes can provide noncharged, hydrophilic, and highly hydrated surfaces to resist cell adhesion;[37−39] on the other hand, PEG chains show the tendency to interact with phosphatidylserine that is in the inner leaflet of normal cell membranes but becomes exposed in abnormal or apoptotic cell membranes,[40,41] resulting in adhesion of dysfunctional cells on PEG brushes. In addition, because the response of cells to polymer brushes depends on the density and surface structure of polymer brushes, a high density of polymer brushes and well-defined surface structure are highly desired.

Here, we present a facile approach to precisely pattern the surface of SEBS with PEG brushes. SEBS is used as a substrate due to its unique nanostructures, good biocompatibility, and outstanding stability under physiological conditions.[12,38,42] In addition, normal RBCs and lysed RBCs are used as model cells because RBCs are nature's long-circulating delivery vehicles implementing many important biological functionalities.[43,44] The strategy is based on the fact that PEG brushes resist normal cell adhesion but promote dysfunctional cell adhesion by preferable interaction with phosphatidylserine exposed on the membrane surface of dysfunctional cells. We demonstrate that varied patterned surfaces, such as positive and negative patterned surfaces, can be obtained by selectively patterning ATRP initiators on the SEBS surface via an aqueous-based method and growing PEG brushes through SI-ATRP. The relatively high initiator density (6.4 initiators/nm^2) and polymerization temperature facilitate formation of PEG brushes in high density, which gives brushes worm-like morphology and superhydrophilic property. The distribution of dysfunctional cells adhered on the patterned surfaces is completely different from well-defined arrays of normal cells on the patterned surfaces, providing a facile method to effectively detect dysfunctional cells. The simplicity and easy handling of the described technique shows the potential application in microdiagnostic devices.

2. EXPERIMENTAL SECTION

2.1. Materials. SEBS copolymer with 29 wt % styrene (Kraton G 1652, M_n = 74800) was purchased from Shell Chemicals (USA). Poly(ethylene glycol) methyl ether methacrylate (OEGMA) monomer ($M_n \approx 475$) and copper(I) bromide (CuBr, 98%) were obtained from Sigma-Aldrich. 2,2′-Bipyridine (Bpy, > 99%) was purchased from Alfa Aesar. OEGMA was passed through a silica gel column to remove the inhibitor and stored under an argon atmosphere at −4 °C. 3-*sn*-Phosphatidyl-L-serine (PS, ≥97%) from bovine brain was purchased from Sigma-Aldrich, and PS labeled with red fluorescent rhodamine B isothiocyanate (RBITC-PS) was obtained from Beijing Biosynthesis Biotechnology Co., Ltd. (China). Dulbecco's modified Eagle's medium (DMEM) and 0.25 wt % trypsin were purchased from Beijing Solarbio Science & Technology. Sterile filtered fetal bovine serum (FBS) was supplied by Beijing Yuanhengjinma Biotechnology. Phosphate-buffered saline (PBS, 0.1 mol/L, pH 7.4) solution was freshly prepared. Other chemicals were analytical grade and used without further purification. Milli-Q water (18.25 MΩcm) was used in all experiments.

2.2. Fabrication of Patterned ATRP Initiator on SEBS. A simple "top-down/bottom-up" strategy was developed to fabricate positive and negative patterned ATRP initiators on the surface of SEBS films. Immobilization of ATRP initiators on the SEBS surface was carried with an aqueous-based method,[38] and the copper grids with different mesh sizes were used as photomasks. For fabricating the positive patterned ATRP initiators, SEBS films incorporating copper grids were exposed to UV/O_3 for 30 min in a cleaning chamber and subsequently immersed in HBr/H_2SO_4 (5/1, v/v) mixture solution for 24 h at 60 °C. Then these treated films were washed drastically with deionized water to remove physically adsorbed HBr and dried overnight under vacuum at 25 °C. The so-obtained films with immobilized patterned initiator were referred to as positive patterned SEBS-Br samples. For fabricating the negative patterned ATRP initiators, the virgin SEBS films were subjected to UV/O_3 for 30 min followed by a subsequent reaction in the HBr/H_2SO_4 (5/1, v/v) mixture solution for 24 h at 60 °C. Then the photomask was positioned on the SEBS-Br surface and exposed to the UV/O_3 treatment for 60 min. Afterward, the treated film was washed drastically with deionized water and dried overnight under vacuum at 25 °C before use. The so-obtained films with immobilized patterned initiator were referred to as negative patterned SEBS-Br samples.

2.3. Formation of Patterned Surfaces with PEG Brushes. The positive and negative patterned surfaces were fabricated with well-defined PEG brushes via SI-ATRP method. The general SI-ATRP procedure is described in detail elsewhere,[38] and only a short description is given here. Briefly, CuBr (63.6 mg, 0.44 mmol), Bpy (150.0 mg, 0.96 mmol), and patterned SEBS-Br samples were placed in a 100 mL round-bottom flask. Oxygen-free conditions were ensured by working in an argon atmosphere. A 70 mL amount of deoxygenated aqueous monomer solution (volumetric ratio of PEG/H_2O equals 1:6) was introduced into the flask under argon protection. The resultant mixture was degassed through three freeze−pump−thaw cycles before the reaction started. The grafting process proceeded at 60 °C for 2h. After reaction, substrates were removed from the polymerization solution, exhaustively rinsed with Milli-Q water to remove all traces of the polymerization solution, and subsequently dried under vacuum overnight at 25 °C.

2.4. Characterization. *2.4.1. XPS Measurements.* The surface composition was determined via X-ray photoelectron spectroscopy (XPS) using a VG Scientific ESCA MK II Thermo Avantage V 3.20 analyzer with Al/K ($h\nu$ =1486.6 eV) anode mono-X-ray source. All samples were completely vacuum dried before characterization. The takeoff angle for the photoelectron analyzer was fixed at 90°. All binding energy (BE) values were referenced to the C_{1s} hydrocarbon peak at 284.6 eV. Atomic concentrations of the elements were calculated by their corresponding peak areas.

2.4.2. ATR-FTIR Measurements. ATR-FTIR measurements of virgin SEBS and grafted films were performed on a Bruker FTIR spectrometer Vertex 70 equipped with an attenuated total reflection (ATR) unit (ATR crystal 45°) at a resolution of 4 cm^{-1} for 32 scans.

2.4.3. SEM. The surface of the film was observed with field emission scanning electron microscopy (FESEM) using a XL 30 ESEM FEG (FEI Co.) instrument equipped with an EDX spectroscopy attachment.

2.4.4. Microscopy. The morphologies of the patterned surface were observed by polarized optical microscopy (Zeiss Axio Imager A2m, Carl Zeiss, Germany) equipped with a video CCD camera.

2.4.5. CLSM. Images were acquired using a confocal laser scanning microscope (CLSM) (LSM700-Zeiss, Germany) equipped with an InGaN semiconductor laser (405 nm), an Ar laser (488 nm), and a He−Ne laser (555 nm). All samples were visualized using the same acquisition settings and analyzed using Zen 2011 software (Carl Zeiss).

2.4.6. Contact Angle Measurements. Surface wettability of unmodified and PEG-modified SEBS was evaluated by the sessile drop method with a pure water droplet (ca. 3 μL) using a contact angle goniometer (DSA, KRUSS GMBH, Germany). The average value of five measurements made at different surface locations on the same sample was adopted as the contact angle.

2.5. Normal RBCs Adhesion. Micropatterned samples were placed into cell culture plates and equilibrated with isotonic saline for

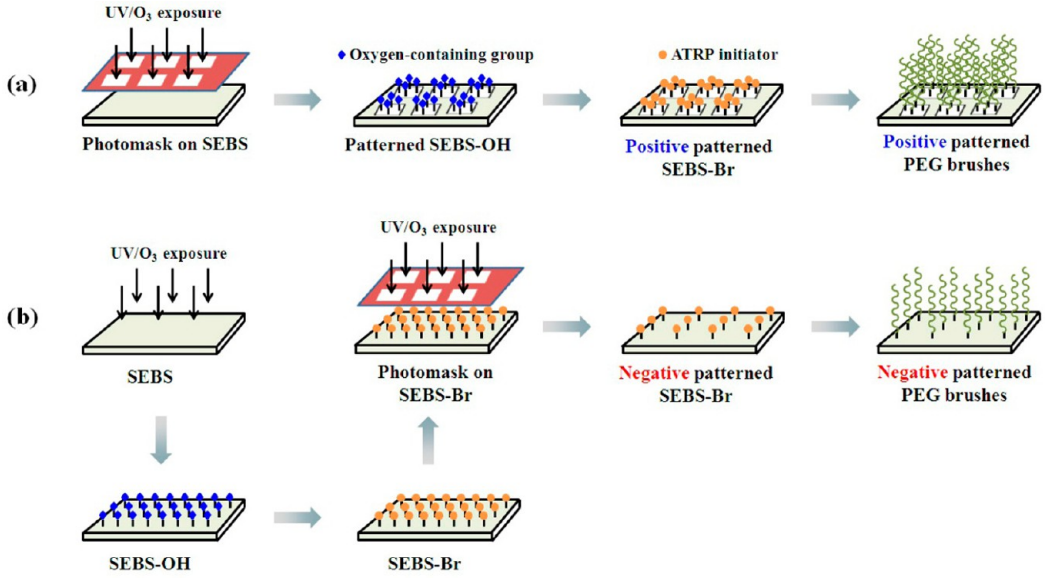

Figure 1. Schematic procedure for fabricating positive and negative patterned surfaces. (a) UV/O_3 irradiation is applied through a photomask to produce oxgen-containing groups on UV/O_3-exposed areas, and these groups are substituted by bromine (Br) in HBr/H_2SO_4 solution, resulting in a positive pattern of ATRP initiators. (b) SEBS film is irradiated by UV/O_3 and treated in HBr/H_2SO_4 solution, followed by selectively etching with UV/O_3 through the photomask to form a negative pattern of ATRP initiators. Then PEG brushes grow from the initiators immobilized on the SEBS surface via SI-ATRP to form positive and negative patterns.

1 h at 37 °C. Fresh blood from healthy white rabbits was extracted via venipuncture through a 19-gauge Butterfly needle into a standard blood collection tube containing 3.8 wt % sodium citrate [9:1 (v/v) blood/anticoagulant]. To isolate and purify the red blood cells (RBCs), we used the method described by Brooks et al.[45] Briefly, the whole blood sample was centrifuged at 1000 rpm (or equivalent to approximately 91 g-force) for 15 min to obtain the RBCs concentrates. Then the RBCs concentrates were washed three times with isotonic saline [0.9% (w/v) of aqueous NaCl solution, pH 7.4]. Subsequently, the RBC pellets were resuspended in normal saline to obtain a RBC suspension at 20% (v/v) hematocrit. Afterward, 80 μL of RBC suspension was dropped on the micropatterned substrate surface and incubated at 37 °C for 60 min under static conditions. After incubation, samples were carefully rinsed twice with prewarmed isotonic saline, followed by fixing with 2.5 vol % glutaraldehyde for 2 h at 4 °C. Finally, samples were freeze dried and the adhered RBCs on the micropatterned sample surfaces were visualized by FESEM and CLSM, respectively.

2.6. Detection of Dysfunctional RBCs. The normal RBCs were incubated in the hypotonic saline [0.3% (w/v)] at room temperature for 1 h to become hemolysis with hemolysis ratio of about 100%. The lysed RBCs are used as model cells for dysfunctional RBCs. Adhesion of dysfunctional RBCs on patterned surface was performed according to the procedure described in normal RBCs adhesion.

2.7. Phosphatidylserine Adsorption. RBITC-PS was dissolved in PBS at a concentration of 1 mg/mL, and the patterned SEBS-*g*-PEG substrates were incubated in the as-prepared RBITC-PS solution for 60 min at 37 °C in the dark. Following incubation, RBITC-PS solutions were removed and the samples were gently washed twice with prewarmed PBS (37 °C). Then the samples were dried under a stream of nitrogen, and fluorescence images were observed with a CLSM (LSM700-Zeiss, Germany). As for the characterization of CLSM, the RBITC dye was excited with an argon ion laser at 555 nm.

2.8. HeLa Cells Attachment Assay. Cell attachment assay was studied using HeLa cells (human cervix epithelial cell line). Cells were maintained on tissue culture plate (TCP) in DMEM supplemented with 4.5 g/L glucose, 10 vol % FBS, 100 units/mL penicillin, and 100 μg/mL streptomycin at 37 °C in a humidified atmosphere of 5 vol % CO_2 and 95 vol % air. After the cells were grown until >90% confluence, the TCP was gently washed once with PBS, and then the floating and loosely attached cells were collected and resuspended with FBS-free DMEM medium after centrifugation. Obtained cells were referred to as dysfunctional cells. Meanwhile, the well-grown cells were trypsinized in a 0.25% (m/m) trypsin solution and detached from the TCP, and the cell suspension was transferred to a tube and centrifuged. After removal of the trypsin, the remaining cells were resuspended with FBS-free DMEM medium and are referred to as normal cells.

The nonpatterned SEBS-*g*-PEG samples with a diameter of 11 mm were pretreated with 75 vol % ethanol aqueous solution for 1 h and followed by extensive rinsing in PBS before immersing in the FBS-free DMEM medium for 1 h. Normal and dysfunctional HeLa cells were seeded onto the samples at a density of 3×10^4 cells/well and incubated at 37 °C under a 5 vol % CO_2 humidified atmosphere. Cells were allowed to adhere to the sample surfaces for 1 h, and phase-contrast images of the cells were taken using an inverted microscope (TE2000-U, Nikon). To quantify cell adhesion, more than five images were obtained for each sample and the images were analyzed with ImageJ software to determine average cell density adhered on the sample surfaces.

3. RESULTS AND DISCUSSION

The 3D patterned SEBS surfaces are created based on a "top-down/bottom-up" strategy (Figure 1) in which creation of ATRP initiators on the SEBS surface is obtained by UV/O_3 irradiation through a photomask and HBr/H_2SO_4 treatment followed by growth of POEGMA brushes from prepatterned ATRP initiators via SI-ATRP. In this work, POEGMA brushes are expressed by PEG brushes for simplicity. TEM grids with different mesh sizes are used as photomasks. In addition, varied surfaces, such as positive and negative patterned surfaces, can be obtained with this strategy, demonstrating the versatility of this method in surface patterning.

3.1. Inverted Patterns of ATRP Initiators. Similar approaches are used to fabricate positive and negative patterns of initiators on the SEBS surface (Figure 1). SEBS films are irradiated by UV/O_3 at room temperature with and without a photomask, followed by immersion of films in HBr/H_2SO_4 mixture solution. Because UV/O_3 irradiation produces oxygen

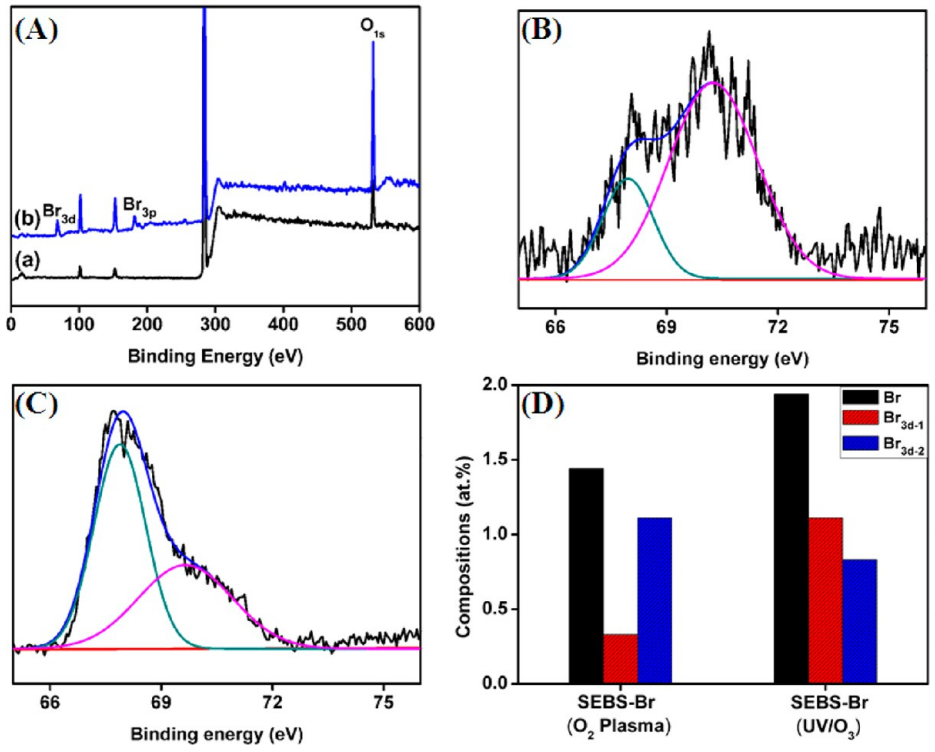

Figure 2. (A) Wide-scan spectra of virgin SEBS (a), SEBS-Br prepared by UV/O_3 treatment (b); (B) Br_{3d} core-level spectrum of the SEBS-Br surface produced by O_2 plasma treatment; (C) Br_{3d} core-level spectrum of the SEBS-Br surface produced by UV/O_3 treatment; (D) Br, Br_{3d-1}, and Br_{3d-2} concentration of the SEBS-Br surfaces produced by O_2 plasma and UV/O_3 treatment.

groups on the UV/O_3-exposed areas[46,47] and these groups are easily substituted by Br atoms in HBr/H_2SO_4 mixture solution,[38] a positive pattern of ATRP initiators is created on the UV/O_3-exposed areas (Figure 1a). Meanwhile, the SEBS film with uniform initiators on its surface is covered by the photomask and exposed to UV/O_3 irradiation again. Due to the etching of initiators on UV-exposed areas, a negative pattern of ATRP initiator is generated on UV-unexposed areas (Figure 1b). Creation of ATRP initiators on the SEBS surface with an aqueous-based method avoids the swelling or dissolution of the underlying substrate caused by use of organic solvents.

Immobilization of ATRP initiators onto the SEBS surface is confirmed by XPS detection. Figure 2A presents XPS wide-scan spectra of virgin SEBS and brominated SEBS (SEBS-Br) surfaces. All survey spectra display a carbon peak (C_{1s}) at 285 eV and oxygen signal (O_{1s}) at 533 eV. In the wide-scan spectrum of SEBS-Br sample, the presence of the O_{1s} peak mainly results from the existence of oxygen-containing groups arising from UV/O_3 treatment, while the oxygen signal of the SEBS surface is due to the oxygen contamination species.[48] In comparison with the spectrum of SEBS, bromine signal (Br_{3d} at ca. 70 eV and Br_{3p} at ca. 180 eV) is detected on the SEBS-Br surface,[49] indicating that the initiator has been successfully introduced on the sample surface.

The initiation sites play a very important role in achieving the high and even surface coverage of the SEBS surface with the functional polymer brushes. In addition, the C−Br bonds directly connecting with the benzene rings of styrene blocks are effective initiation sites for SI-ATRP.[50] In order to compare the initiator density with our previous work, in which the ATRP initiators are created by the combination of O_2 plasma irradiation and bromination,[38] the initiator density is quantitatively evaluated by Br content in XPS spectra. XPS spectra of SEBS-Br samples produced by O_2 plasma and UV/O_3 irradiation are displayed in Figure 2B and 2C, respectively. In both cases, the Br_{3d} peak can be curved into two main components with binding energies of about 67.9 (Br_{3d-1}) and 70.2 eV (Br_{3d-2}) based on XPS peak-differentiating software. The former is attributed to C−Br species connecting with benzene rings of styrene blocks (effective initiator),[51] while the latter is attributed to C−Br species connecting with aliphatic blocks. For the SEBS-Br sample produced by O_2 plasma treatment it has a main peak at 70.2 eV (Br_{3d-2}) and a shoulder peak at 67.9 eV (Br_{3d-1}); in contrast, the peak at 67.9 eV (Br_{3d-1}) becomes the main peak for the SEBS-Br sample produced by UV/O_3 treatment. Figure 2D shows the surface concentration of the Br atom and composition of Br_{3d-1} and Br_{3d-2} (in atom %) obtained by integration of the core level peaks. The bromine content of the SEBS-Br surface (UV/O_3 treatment) increases up to 1.94%, while the bromine content of the SEBS-Br surface (O_2 plasma treatment) is just 1.44% (~4.76 initiators/nm^2).[38] From the results discussed above, the initiator density for the SEBS-Br surface prepared by UV/O_3 treatment is estimated to be about 6.4 initiators/nm^2. Furthermore, the Br_{3d-1} content of the former (1.11%) is three times more than the latter (0.33%). Thus, the density of effective initiation sites is much higher than that of initiators on SEBS generated with treatment of O_2 plasma.

3.2. Formation of Superhydrophilic PEG Brushes with Wormlike Morphology. PEG brushes are then formed via SI-ATRP from the model surfaces. Formation of polymer brushes is analyzed with ATR-FTIR spectra (Figure 3). Compared with the spectrum of the virgin SEBS surface (Figure 3a), all grafted samples show two intense bands at 1728 and 1110 cm^{-1} (Figure 3b−d), characteristic of the stretching vibration of C═O and C−O−C, respectively.[36] Moreover, the peaks at

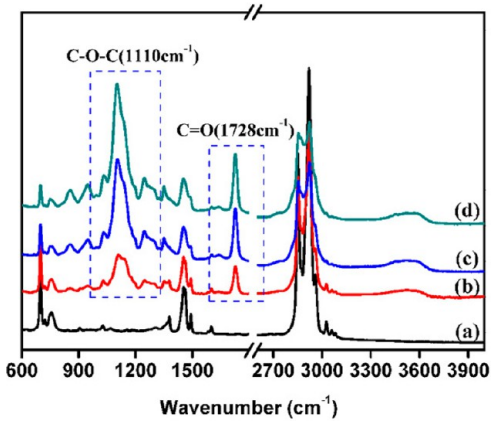

Figure 3. ATR-FTIR spectra of the surfaces of (a) pristine SEBS, (b) SEBS-*g*-PEG prepared at 40 °C with a $Br_{3d\text{-}1}$ concentration of 0.33%, (c) SEBS-*g*-PEG prepared at 40 °C with a $Br_{3d\text{-}1}$ concentration of 1.11%, and (d) SEBS-*g*-PEG prepared at 60 °C with a $Br_{3d\text{-}1}$ concentration of 1.11%. All ATRP processes are performed for 10 h.

1349 and 1288 cm^{-1}, which are attributed to antisymmetric OCH_2-CH_2 stretching and symmetric OCH_2-CH_2 stretching, are clearly observed.[52] These results provide direct evidence that the PEG brushes have been successfully grafted onto the SEBS surface.

The effects of effective initiator density and temperature on grafting density of PEG brushes are also investigated. The intensity of peaks at 1110 and 1728 cm^{-1} for the formed PEG brushes in Figure 3c (with $Br_{3d\text{-}1}$ concentration of 1.11%) is much stronger than that of Figure 3b (with $Br_{3d\text{-}1}$ concentration of 0.33%), indicating a high effective initiator density facilitates a high grafting density of PEG brushes. Grafting of PEG brushes from the surface with a $Br_{3d\text{-}1}$ concentration of 1.11% is carried out at 40 and 60 °C. The intensities of the C═O and C−O−C peaks of PEG brushes performed at 60 °C are much higher than that performed at 40 °C, indicating a higher reaction temperature results in a higher grafting density of PEG brushes.

The dependence of the surface properties of PEG brushes on initiator density and reaction temperature is further analyzed by SEM and water contact angle measurements (Figure 4). Figure 4a shows that the surface of virgin SEBS film is relatively flat and quite hydrophobic with a contact angle of 105°. No obvious difference in the morphology is observed on the grafted surface performed at 40 °C with low initiator density (with $Br_{3d\text{-}1}$ concentration of 0.33%), but a decrease in the water contact angle (CA, 48°) is obtained due to the inherent hydrophilic nature of PEG brushes (Figure 4b).[53,54] The grafted surface with a high initiator density (with a $Br_{3d\text{-}1}$ concentration of 1.11%) becomes relatively rough with irregularly packed convex papillae (asperities) (Figure 4c), and the contact angle (46°) is similar to that on the SEBS surface with low initiator density. The hierarchical and irregular wormlike structures of PEG brushes appear on the surface of UV/O_3-treated SEBS with a grafting temperature of 60 °C (Figure 4d). Entanglement of PEG brushes results in high thickness and porous structures of brushes (see Figure S1, Supporting Information), which renders the surface superhydrophilic (see Supporting Information, Video S1). Therefore, both the high initiator density and the reaction temperature lead to a high grafting density and thickness of PEG brushes, which exhibit unique superhydrophilic property and wormlike morphology structure compared with the hydrophilicity and surface structure of PEG brushes reported by other works.[55,56]

3.3. Formation of Positive and Negative Patterns via SI-ATRP. Figure 5 shows optical and SEM images of positive and negative patterns on the SEBS surface after grafting PEG

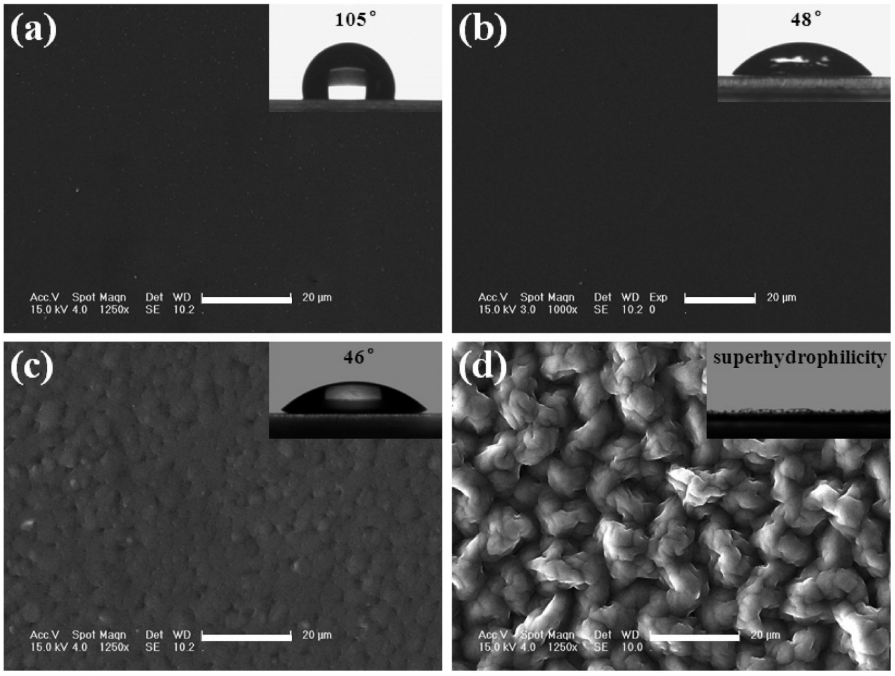

Figure 4. SEM images and water contact angle on virgin and grafted SEBS: (a) virgin SEBS surface, (b) SEBS-*g*-PEG surface prepared under ATRP conditions (10 h, 40 °C) with a $Br_{3d\text{-}1}$ concentration of 0.33%, (c) SEBS-*g*-PEG surface prepared under ATRP conditions (10 h, 40 °C) with a $Br_{3d\text{-}1}$ concentration of 1.11%, (d) SEBS-*g*-PEG surface prepared under ATRP conditions (10 h, 60 °C) with a $Br_{3d\text{-}1}$ concentration of 1.11%. Scale bar is 20 μm in all images.

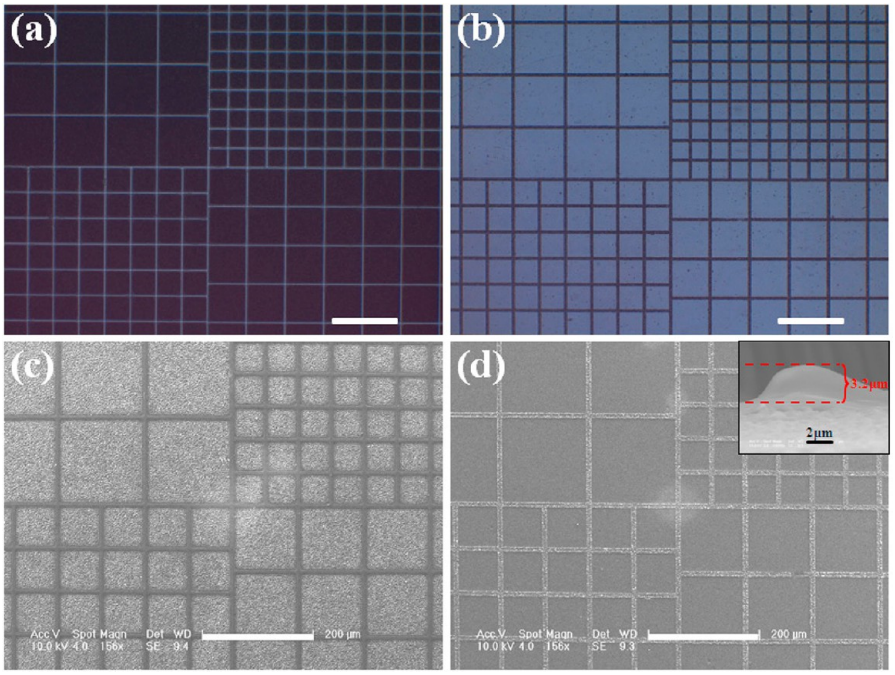

Figure 5. Optical images (a, b) and SEM images (c, d) of positive (a, c) and negative (b, d) patterned surface. Scale bar is 200 μm in all images. (Inset of d) SEM image of the cross section of PEG brushes with high magnification.

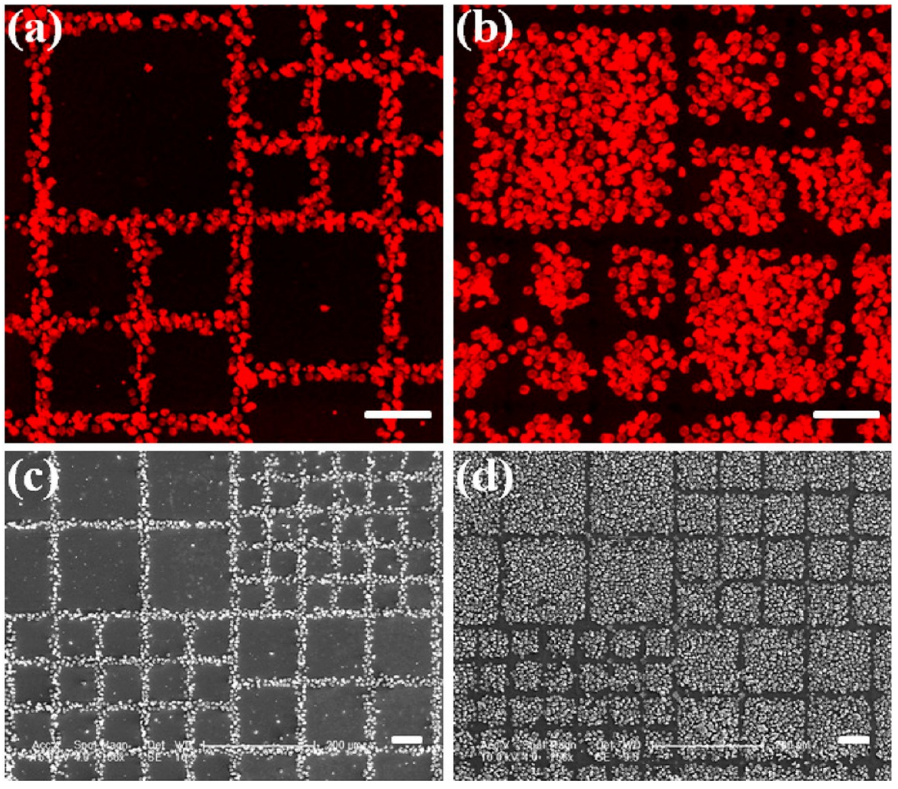

Figure 6. CLSM (a, b) and SEM (c, d) images showing the RBC microarrays on the positive (a, c) and negative (b, d) patterned surfaces. Scale bar is 50 μm in all images.

brushes atop the ATRP initiator layer. Optical images of the positive patterned surface show generation of PEG brushes on one surface with different square sizes ranging from 52 to 155 μm (Figure 5a). The dark squares are covered with PEG brushes because PEG brushes selectively grow on the UV/O_3-irradiated areas. A typical SEM image of the positive patterned surface shows that the homogeneous polymer brushes are closely packed, and the roughness on the square parts is much higher than that on the line parts (Figure 5c). Optical and SEM images of the negative patterned surface are shown in Figure 5b and 5d, respectively. Polymer brushes are grown in line parts, which are complementary to that grown on a positive pattern

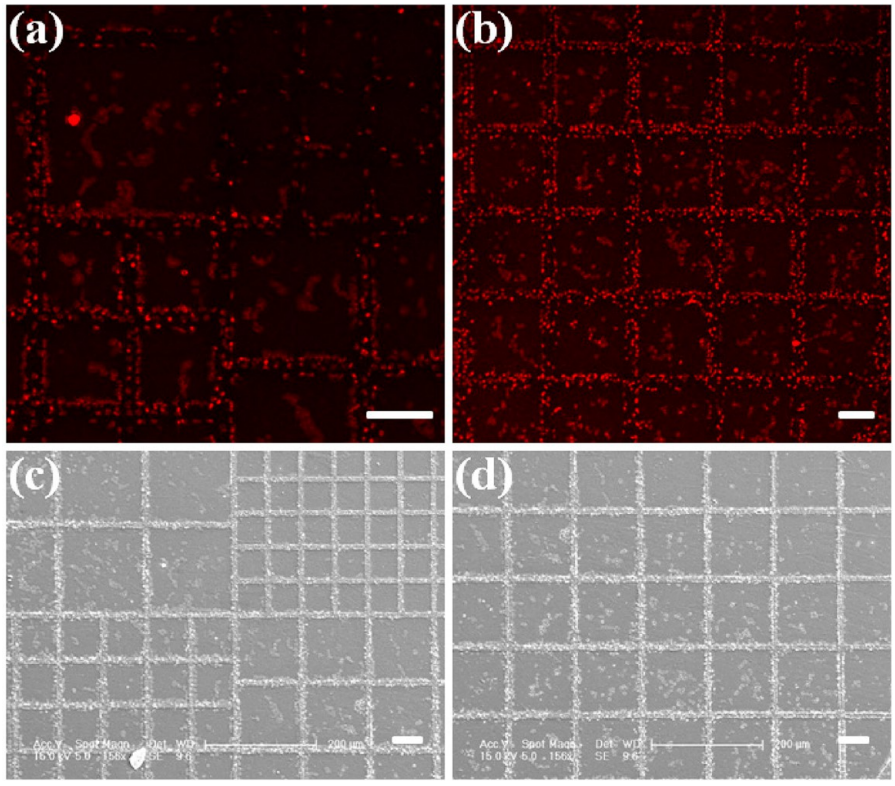

Figure 7. CLSM (a, b) and SEM (c, d) images showing the dysfunctional RBCs adhesion on the negative patterned surfaces. Scale bar is 50 μm in all images.

surface. The inset of Figure 5d shows the SEM image of the cross section of the negative patterned SEBS-*g*-PEG surface. It is clearly seen that the thickness of the PEG brushes is about 3.2 μm. These results illustrate that both a positive and a negative 3D patterned surface have a uniform and closely packed structure with high lateral resolution, indicating this method allows fabricating patterned surfaces with tunable chemistry and size of the microscopic features.

3.4. Normal RBCs Adhesion and Dysfunctional RBCs Detection. Patterned surfaces provide powerful tools to control cell adhesion and array. Here, normal red blood cells (RBCs) are selected as model cells to perform cell patterning, because RBCs are nature's long-circulating delivery vehicles implementing many important biological functionalities, such as transport of oxygen and nutrients, coagulation for hemostasis, and immunoprotection.[43,44] Figure 6 shows CLSM and SEM images of adhered normal RBCs on the inverted patterned surfaces. Interestingly, red fluorescent RBCs can be observed by CLSM after excitation at 555 nm, and RBCs exhibit biconcave morphology (Figure 6a and 6b).

For the positive patterned surface, RBCs selectively adhere along the line parts of the pattern, whose width (13 μm) is just larger than the size of RBC (8 μm). For the negative patterned surface, RBCs are firmly attached on square parts, which is completely adverse to cell arrays on positive patterned surface. Cells adhere in a controlled manner according to the pattern of surface, which consists of many squares with different sizes (Figure 6b and 6d). This phenomenon is well understood as grafted PEG brushes provide a strong hydration layer present on the substrate surface to resist cell adhesion;[58,59] the cell microarrays are mainly caused by the hydrophobic interaction between the underlying SEBS substrate and the cell membranes.

Sickle cell disease, blood transfusion, and sepsis often lead to hemolysis to generate dysfunctional RBCs.[60] Hemolysis is the dissolution of RBCs with the release of intracellular hemoglobin, which reduces oxygen affinity and delivery, causing an intrinsic mechanism for human disease.[61,62] Thus, direct detection of lysed RBCs from blood is important to diagnose and treat diseased RBCs. In this work, the lysed RBCs are obtained by pipetting the RBCs into hypotonic saline [0.3% (w/v)] to model dysfunctional cells. In addition, patterned surfaces are used as simple and user-friendly platforms to detect dysfunctional RBCs. The typical images (CLSM and SEM) of dysfunctional RBCs adhered on negative patterned surface are shown in Figure 7.

In comparison with the cell microarrays of normal RBCs adhesion (Figure 6b), the distribution of adhered dysfunctional RBCs appears disordered (Figure 7a). In addition, the majority of dysfunctional cells tend to adhere onto the line parts where it is fully populated with polymer chains (Figure 7b). The red fluorescence density of lysed RBCs is much weaker than that of normal RBCs under the same viewing conditions, which may be caused by the loss of hemoglobin in lysed RBCs. In comparison with the biconcave discs of normal RBCs (see Figure S2a, Supporting Information), the dysfunctional RBCs exhibit irregular flat discs (see Figure S2b, Supporting Information). Becuase phosphatidylserine becomes exposed on the membrane surface of lysed RBCs[40] and the phosphatidylserine tends to interact with PEG brushes,[41] adhesion of dysfunctional RBCs onto PEG brushes is obtained. Similar results are observed on the positive patterned surfaces (see Figure S3, Supporting Information).

Figure 8 displays the statistical results of normal and dysfunctional RBCs adhered on the SEBS region and the PEG region. The density of normal RBCs adhered on the PEG

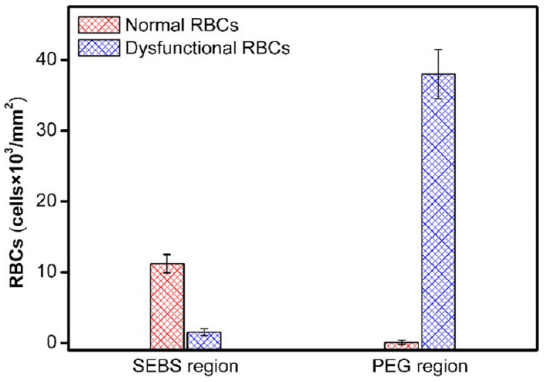

Figure 8. Statistical number of normal and dysfunctional RBCs adhered on the SEBS region and PEG region. Error bars represent a standard deviation for $n = 5$.

region (~78 cells/mm^2) is much lower than that adhered on the SEBS region (~11.2 × 10^3 cells/mm^2), which is due to the fact that highly hydrated PEG chains in water can strongly repel cells approaching the substrate surface. As for dysfunctional RBCs, there is an average of (1.5 ± 0.3) × 10^3 cells/mm^2 on the SEBS region and (38.2 ± 3.5) × 10^3 cells/mm^2 on the PEG region, respectively. The former is mainly caused by the hydrophobic interaction between SEBS substrate and dysfunctional RBCs membranes, while the latter is expected to result from the interactions between PEG and phosphatidylserine (PS), a cell membrane component present in the inner leaflet of normal cells and becomes exposed in abnormal or apoptotic cells. The interaction between PEG and PS is much stronger than the hydrophobic interaction. As hydrophilic PEG brushes prevent damage of captured dysfunctional cells, these abnormal cells can be readily collected for later analysis to investigate their role in disease progression.[11] In addition, the patterned PEG brushes facilitate nonskilled persons to interpret the adhesion results and estimate the content of diseased cells accurately.

3.5. Interaction between Phosphatidylserine and PEG Brushes. To verify the interaction between PS and PEG brushes, adsorption of RBITC-labeled PS (RBITC-PS) on the patterned surfaces is performed. The resultant fluorescence images of positive and negative patterned SEBS-*g*-PEG surfaces before and after RBITC-PS adsorption are shown in Figure 9. The patterned surfaces do not show any fluorescence in the detection wavelength range of RBITC (Figure 9a and 9b). In contrast, spatially well-ordered, two-dimensional RBITC-PS patterns appear on the surfaces with fluorescence intensity (Figure 9a′ and 9 b′). The fluorescence intensity indicates the high density of adsorbed PS. Thus, these results provide direct evidence that there is an interaction between PEG brushes and PS, and the interaction is much higher than the hydrophobic interaction between PS and SEBS substrate.

To widen the application of this platform, HeLa cell attachment is performed. It is well established that HeLa cells exhibit high levels of PS exposure during apoptosis.[63,64] Figure 10 shows the attachment of normal and dysfunctional HeLa

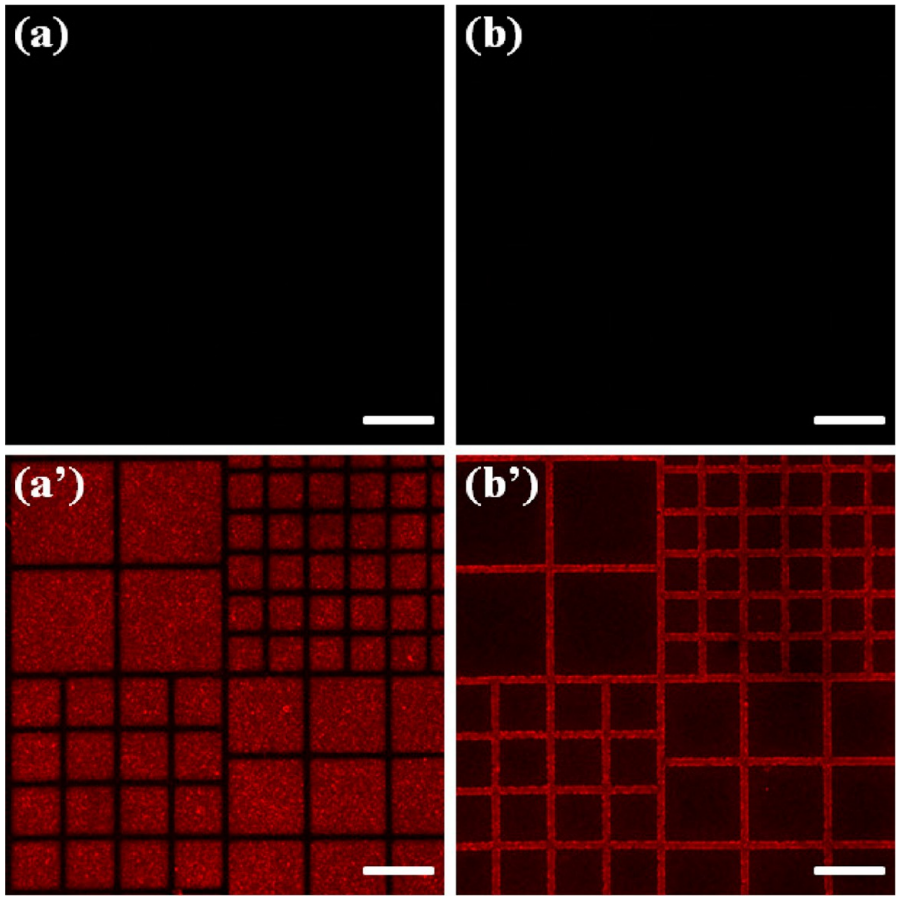

Figure 9. Fluorescent images of positive (a, a′) and negative (b, b′) patterned SEBS-*g*-PEG surfaces before (a, b) and after (a′, b′) RBITC-PS adsorption. Scale bar is 100 μm in all images.

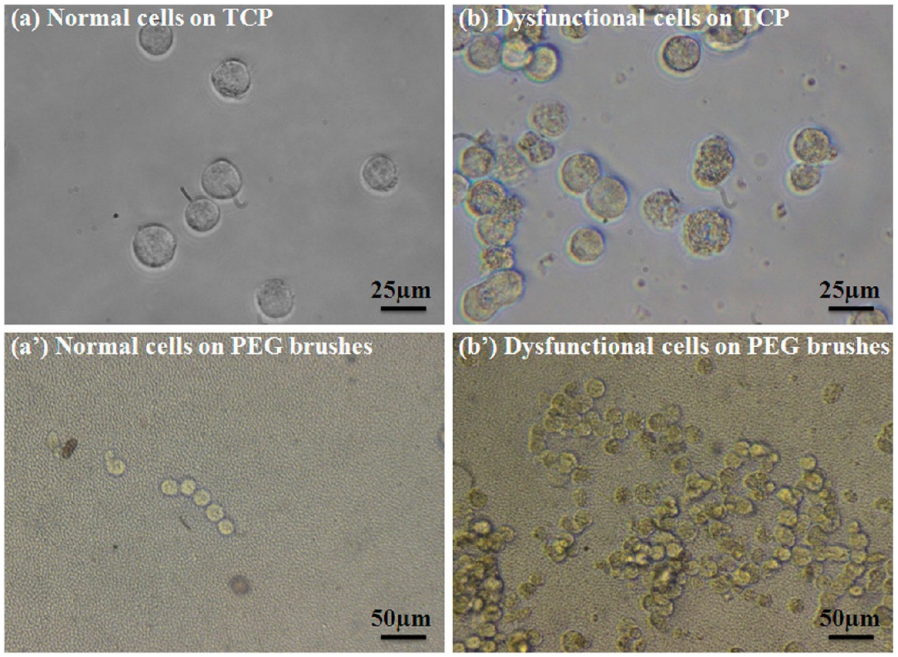

Figure 10. Optical micrographs showing the attachment of normal and dysfunctional HeLa cells onto TCP and PEG brushes.

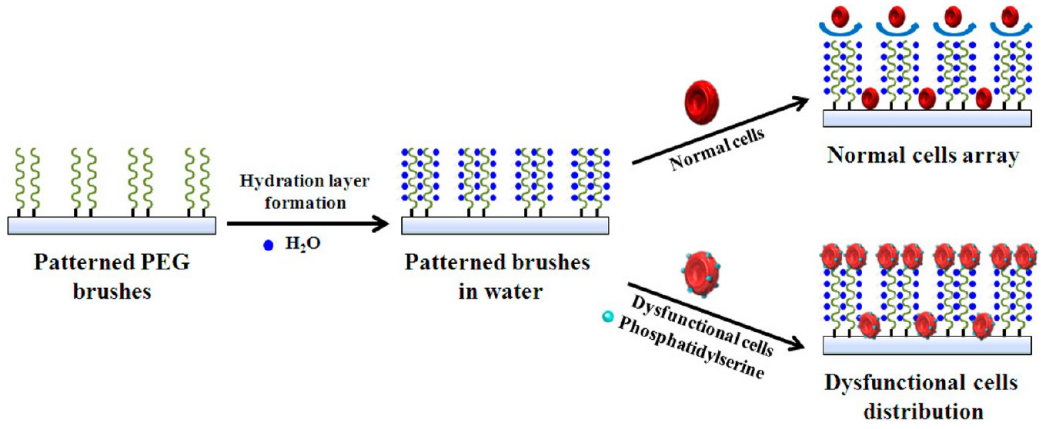

Figure 11. Mechanism for normal and dysfunctional cells detection on the patterned surfaces.

cells onto TCP and PEG brushes. Compared with normal cells (Figure 10a), the dysfunctional cells display typical apoptosis features such as chromatin condensation, membrane disintegration, nuclear fragmentation, and apoptotic bodies (Figure 10b). Figure 10a′ shows that there are few normal cells adhered on the PEG brushes because the highly hydrated PEG chains strongly repel cell adhesion on the substrate surface. In contrast, the number of captured dysfunctional cells is drastically increased on the PEG brushes (Figure 10b′). The comparison of the statistical number of adhered normal and dysfunctional HeLa cells onto PEG brushes is clearly exhibited in Figure S4 (Supporting Information). The above results indicate that the PEG patterned surfaces can be used to detect abnormal and apoptotic cells through the interaction between PEG and phosphatidylserine exposed on the membrane surface of dysfunctional cells.

3.6. Mechanism for Normal and Dysfunctional Cells Detection on the Patterned Surfaces. The mechanism for normal and dysfunctional cells detection on the patterned surface is shown in Figure 11. Once the substrate with patterned PEG brushes contacts water, water molecules likely form hydrogen bonds with two adjacent oxygens of the monomer unit of PEG and thus stabilize the water interface with helical PEG brushes.[65] When the patterned surface contacts normal cells, the presence of water molecules within the PEG brushes and the flexibility of highly hydrated chains can effectively repel the cells approaching the substrate surface. The cell microarrays are thus formed on the regions without PEG brushes, which is mainly caused by the hydrophobic interaction between the underlying SEBS substrate and cell membranes. Because phosphatidylserine becomes exposed at the external surface of the dysfunctional cells[40,66] and the phosphatidylserine interacts with PEG brushes,[41] the dysfunctional cells are effectively detected with PEG brushes in a harmless manner.

It is obvious that the patterned surface with PEG brushes provides a facile and user-friendly platform in effectively detecting abnormal and apoptotic cells without harm to detected cells. As a prepattern of initiators can be performed on widely used substrates and the structure and morphology of PEG brushes can be precisely controlled, the method presented here is universal to construct a platform to detect dysfunctional

and aging cells. The simplicity and easy handling of the described technique shows potential application in microdiagnostic devices.

4. CONCLUSIONS

In this work, we presented a facile method to construct varied 3D patterns on the SEBS surface with PEG brushes in order to develop a portable and user-friendly platform for dysfunctional cell detection. Normal red blood cells (RBCs) and lysed RBCs (dysfunctional cells) were used as model cells. The strategy was based on the fact that PEG brushes tended to interact with phosphatidylserine, which was in the inner leaflet of normal cell membranes but became exposed in abnormal or apoptotic cells. We demonstrated that varied patterned surfaces could be obtained by combination of selectively patterning ATRP initiators on SEBS surfaces and controlled growth of PEG brushes through SI-ATRP. The relatively high initiator density and polymerization temperature resulted in formation of PEG brushes in high density, which gave brushes worm-like and porous structure with superhydrophilic property. The tendency of dysfunctional cells adhered on the PEG brushes was completely different from well-defined arrays of normal cells on the patterned surfaces, providing a facile method to detect dysfunctional cells effectively. The simplicity and easy handling of the described technique showed potential application in microdiagnostic devices.

■ ASSOCIATED CONTENT

Supporting Information

SEM images of the as-grown PEG brushes with different magnifications; video clip showing absorption of water droplets on the superhydrophilic PEG brushes; SEM images showing cellular morphologies of adhered normal RBCs and dysfunctional RBCs; representative CLSM images for dysfunctional RBCs adhesion on the positive micropatterned surfaces. This material is available free of charge via the Internet at http://pubs.acs.org.

■ AUTHOR INFORMATION

Corresponding Authors

*E-mail: shiqiang@ciac.ac.cn.
*E-mail: yinjh@ciac.ac.cn.

Notes

The authors declare no competing financial interest.

■ ACKNOWLEDGMENTS

This work was supported by the financial support of the National Natural Science Foundation of China (Project Nos. 51273199, 21274150, and 51103030). The authors are grateful to Dr. Yuan Lin and Dr. Bo Wang for their assistance in performing HeLa cells attachment assay and helpful discussions.

■ REFERENCES

(1) Cheung, R. K.; Utz, P. J. Screening: CyTOF-The Next Generation of Cell Detection. *Nat. Rev. Rheumatol* **2011**, *7*, 502−503.
(2) Bhadra, R.; Gigley, J. P.; Weiss, L. M.; Khan, I. A. Control of Toxoplasma Reactivation by Rescue of Dysfunctional CD8+ T-cell Response via PD-1−PDL-1 Blockade. *Proc. Natl. Acad. Sci. U.S.A.* **2011**, *108*, 9196−9201.
(3) Makowski, M. S.; Ivanisevic, A. Molecular Analysis of Blood with Micro-/Nanoscale Field-Effect-Transistor Biosensors. *Small* **2011**, *7*, 1863−1875.
(4) Ilic, B.; Czaplewski, D.; Zalalutdinov, M.; Craighead, H.; Neuzil, P.; Campagnolo, C.; Batt, C. Single Cell Detection with Micromechanical Oscillators. *J. Vac. Sci. Technol. B* **2001**, *19*, 2825−2828.
(5) Nguyen, T. A.; Yin, T.-I.; Reyes, D.; Urban, G. A. Microfluidic Chip with Integrated Electrical Cell-Impedance Sensing for Monitoring Single Cancer Cell Migration in Three-Dimensional Matrixes. *Anal. Chem.* **2013**, *85*, 11068−11076.
(6) Racila, E.; Euhus, D.; Weiss, A. J.; Rao, C.; McConnell, J.; Terstappen, L. W.; Uhr, J. W. Detection and Characterization of Carcinoma Cells in the Blood. *Proc. Natl. Acad. Sci. U.S.A.* **1998**, *95*, 4589−4594.
(7) Pantel, K.; Alix-Panabières, C. Circulating Tumour Cells in Cancer Patients: Challenges and Perspectives. *Trends Mol. Med.* **2010**, *16*, 398−406.
(8) Kim, J.-W.; Galanzha, E. I.; Zaharoff, D. A.; Griffin, R. J.; Zharov, V. P. Nanotheranostics of Circulating Tumor Cells, Infections and Other Pathological Features in Vivo. *Mol. Pharmaceutics* **2013**, *10*, 813−830.
(9) Vella, S. J.; Beattie, P.; Cademartiri, R.; Laromaine, A.; Martinez, A. W.; Phillips, S. T.; Mirica, K. A.; Whitesides, G. M. Measuring Markers of Liver Function Using a Micropatterned Paper Device Designed for Blood from a Fingerstick. *Anal. Chem.* **2012**, *84*, 2883−2891.
(10) Shin, D. S.; You, J.; Rahimian, A.; Vu, T.; Siltanen, C.; Ehsanipour, A.; Stybayeva, G.; Sutcliffe, J.; Revzin, A. Photodegradable Hydrogels for Capture, Detection, and Release of Live Cells. *Angew. Chem., Int. Ed.* **2014**, *53*, 8221−8224.
(11) Shah, A. M.; Yu, M.; Nakamura, Z.; Ciciliano, J.; Ulman, M.; Kotz, K.; Stott, S. L.; Maheswaran, S.; Haber, D. A.; Toner, M. Biopolymer System for Cell Recovery from Microfluidic Cell Capture Devices. *Anal. Chem.* **2012**, *84*, 3682−3688.
(12) Ye, W.; Shi, Q.; Wong, S. C.; Hou, J.; Shi, H.; Yin, J. Patterning Surfaces for Controlled Platelet Adhesion and Detection of Dysfunctional Platelets. *Macromol. Biosci.* **2013**, *13*, 676−681.
(13) Ye, W.; Shi, Q.; Wong, S.-C.; Hou, J.; Xu, X.; Yin, J. Precise Patterning of the SEBS Surface by UV Lithography to Evaluate the Platelet Function Through Single Platelet Adhesion. *Biomater. Sci.* **2014**, *2*, 1186−1194.
(14) Ekblad, T.; Faxälv, L.; Andersson, O.; Wallmark, N.; Larsson, A.; Lindahl, T. L.; Liedberg, B. Patterned Hydrogels for Controlled Platelet Adhesion from Whole Blood and Plasma. *Adv. Funct. Mater.* **2010**, *20*, 2396−2403.
(15) Chen, T.; Amin, I.; Jordan, R. Patterned Polymer Brushes. *Chem. Soc. Rev.* **2012**, *41*, 3280−3296.
(16) Hou, J.; Shi, Q.; Ye, W.; Stagnaro, P.; Yin, J. Micropatterning of Hydrophilic Polyacrylamide Brushes to Resist Cell Adhesion but Promote Protein Retention. *Chem. Commun.* **2014**, *50*, 14975−14978.
(17) Steinbach, A.; Tautzenberger, A.; Schaller, A.; Kalytta-Mewes, A.; Tränkle, S.; Ignatius, A.; Volkmer, D. Plasma-Enhanced Chemical Vapor Deposition of n-Heptane and Methyl Methacrylate for Potential Cell Alignment Applications. *ACS Appl. Mater. Interfaces* **2012**, *4*, 5196−5203.
(18) Rodriguez - Emmenegger, C.; Preuss, C. M.; Yameen, B.; Pop - Georgievski, O.; Bachmann, M.; Mueller, J. O.; Bruns, M.; Goldmann, A. S.; Bastmeyer, M.; Barner - Kowollik, C. Controlled Cell Adhesion on Poly(dopamine) Interfaces Photopatterned with Non-Fouling Brushes. *Adv. Mater.* **2013**, *25*, 6123−6127.
(19) Crouzier, T.; Jang, H.; Ahn, J.; Stocker, R.; Ribbeck, K. Cell Patterning with Mucin Biopolymers. *Biomacromolecules* **2013**, *14*, 3010−3016.
(20) Yu, Q.; Johnson, L. M.; López, G. P. Nanopatterned Polymer Brushes for Triggered Detachment of Anchorage-Dependent Cells. *Adv. Funct. Mater.* **2014**, *24*, 3751−3759.
(21) Yoshimoto, K.; Ichino, M.; Nagasaki, Y. Inverted Pattern Formation of Cell Microarrays on Poly (ethylene glycol) (PEG) Gel Patterned Surface and Construction of Hepatocyte Spheroids on Unmodified PEG Gel Microdomains. *Lab Chip* **2009**, *9*, 1286−1289.
(22) Zhou, X.; Liu, X.; Xie, Z.; Zheng, Z. 3D-Patterned Polymer Brush Surfaces. *Nanoscale* **2011**, *3*, 4929−4939.

(23) Liu, J.-F.; Cruchon-Dupeyrat, S.; Garno, J. C.; Frommer, J.; Liu, G.-Y. Three-Dimensional Nanostructure Construction via Nanografting: Positive and Negative Pattern Transfer. *Nano Lett.* **2002**, *2*, 937−940.
(24) Justice, B. A.; Badr, N. A.; Felder, R. A. 3D Cell Culture Opens New Dimensions in Cell-Based Assays. *Drug Discovery Today* **2009**, *14*, 102−107.
(25) Bajaj, P.; Schweller, R. M.; Khademhosseini, A.; West, J. L.; Bashir, R. 3D Biofabrication Strategies for Tissue Engineering and Regenerative Medicine. *Annu. Rev. Biomed. Eng.* **2014**, *16*, 247−276.
(26) Zhou, X.; Liu, Z.; Xie, Z.; Liu, X.; Zheng, Z. High-Resolution, Large-Area, Serial Fabrication of 3D Polymer Brush Structures by Parallel Dip-Pen Nanodisplacement Lithography. *Small* **2012**, *8*, 3568−3572.
(27) Xie, Z.; Chen, C.; Zhou, X.; Gao, T.; Liu, D.; Miao, Q.; Zheng, Z. Massively Parallel Patterning of Complex 2D and 3D Functional Polymer Brushes by Polymer Pen Lithography. *ACS Appl. Mater. Interfaces* **2014**, *6*, 11955−11964.
(28) Nie, Z.; Kumacheva, E. Patterning Surfaces with Functional Polymers. *Nat. Mater.* **2008**, *7*, 277−290.
(29) Matyjaszewski, K.; Tsarevsky, N. V. Nanostructured Functional Materials Prepared by Atom Transfer Radical Polymerization. *Nat. Chem.* **2009**, *1*, 276−288.
(30) Xu, F.; Neoh, K.; Kang, E. Bioactive Surfaces and Biomaterials via Atom Transfer Radical Polymerization. *Prog. Polym. Sci.* **2009**, *34*, 719−761.
(31) Yan, J.; Li, B.; Yu, B.; Huck, W. T.; Liu, W.; Zhou, F. Controlled Polymer-Brush Growth from Microliter Volumes Using Sacrificial-Anode Atom-Transfer Radical Polymerization. *Angew. Chem., Int. Ed.* **2013**, *52*, 9125−9129.
(32) Ran, J.; Wu, L.; Zhang, Z.; Xu, T. Atom Transfer Radical Polymerization (ATRP): a Versatile and Forceful Tool for Functional Membranes. *Prog. Polym. Sci.* **2014**, *39*, 124−144.
(33) Yang, W. J.; Neoh, K.-G.; Kang, E.-T.; Teo, S. L.-M.; Rittschof, D. Polymer Brush Coatings for Combating Marine Biofouling. *Prog. Polym. Sci.* **2014**, *39*, 1017−1042.
(34) Yah, W. O.; Xu, H.; Soejima, H.; Ma, W.; Lvov, Y.; Takahara, A. Biomimetic Dopamine Derivative for Selective Polymer Modification of Halloysite Nanotube Lumen. *J. Am. Chem. Soc.* **2012**, *134*, 12134−12137.
(35) Coad, B. R.; Lu, Y.; Glattauer, V.; Meagher, L. Substrate-Independent Method for Growing and Modulating the Density of Polymer Brushes from Surfaces by ATRP. *ACS Appl. Mater. Interfaces* **2012**, *4*, 2811−2823.
(36) Siegwart, D. J.; Oh, J. K.; Matyjaszewski, K. ATRP in the Design of Functional Materials for Biomedical Applications. *Prog. Polym. Sci.* **2012**, *37*, 18−37.
(37) Tan, Y. F.; Chandrasekharan, P.; Maity, D.; Yong, C. X.; Chuang, K.-H.; Zhao, Y.; Wang, S.; Ding, J.; Feng, S.-S. Multimodal Tumor Imaging by Iron Oxides and Quantum Dots Formulated in Poly(lactic acid)-D-Alpha-Tocopheryl Polyethylene Glycol 1000 Succinate Nanoparticles. *Biomaterials* **2011**, *32*, 2969−2978.
(38) Hou, J.; Shi, Q.; Stagnaro, P.; Ye, W.; Jin, J.; Conzatti, L.; Yin, J. Aqueous-Based Immobilization of Initiator and Surface-Initiated ATRP to Construct Hemocompatible Surface of Poly(styrene-b-(ethylene-co-butylene)-b-styrene) Elastomer. *Colloids Surf., B* **2013**, *111*, 333−341.
(39) Guo, W.; Zhu, J.; Cheng, Z.; Zhang, Z.; Zhu, X. Anticoagulant Surface of 316 L Stainless Steel Modified by Surface-Initiated Atom Transfer Radical Polymerization. *ACS Appl. Mater. Interfaces* **2011**, *3*, 1675−1680.
(40) Boas, F. E.; Forman, L.; Beutler, E. Phosphatidylserine Exposure and Red Cell Viability in Red Cell Aging and in Hemolytic Anemia. *Proc. Natl. Acad. Sci. U.S.A.* **1998**, *95*, 3077−3081.
(41) Boni, L.; Stewart, T.; Alderfer, J.; Hui, S. Lipid-Polyethylene Glycol Interactions: I. Induction of Fusion between Liposomes. *J. Membr. Biol.* **1981**, *62*, 65−70.
(42) Shi, Q.; Fan, Q.; Ye, W.; Hou, J.; Wong, S.-C.; Xu, X.; Yin, J. Controlled Lecithin Release from a Hierarchical Architecture on Blood-Contacting Surface to Reduce Hemolysis of Stored Red Blood Cells. *ACS Appl. Mater. Interfaces* **2014**, *6*, 9808−9814.
(43) Gao, W.; Hu, C. M. J.; Fang, R. H.; Luk, B. T.; Su, J.; Zhang, L. Surface Functionalization of Gold Nanoparticles with Red Blood Cell Membranes. *Adv. Mater.* **2013**, *25*, 3549−3553.
(44) She, S.; Li, Q.; Shan, B.; Tong, W.; Gao, C. Fabrication of Red-Blood-Cell-Like Polyelectrolyte Microcapsules and Their Deformation and Recovery Behavior Through a Microcapillary. *Adv. Mater.* **2013**, *25*, 5814−5818.
(45) Yu, X.; Zou, Y.; Horte, S.; Janzen, J.; Kizhakkedathu, J. N.; Brooks, D. E. Thermal Reversal of Polyvalent Choline Phosphate, a Multivalent Universal Biomembrane Adhesive. *Biomacromolecules* **2013**, *14*, 2611−2621.
(46) Bhat, R. R.; Chaney, B. N.; Rowley, J.; Liebmann - Vinson, A.; Genzer, J. Tailoring Cell Adhesion Using Surface-Grafted Polymer Gradient Assemblies. *Adv. Mater.* **2005**, *17*, 2802−2807.
(47) Vennerberg, D. C.; Quirino, R. L.; Jang, Y.; Kessler, M. R. Oxidation Behavior of Multiwalled Carbon Nanotubes Fluidized with Ozone. *ACS Appl. Mater. Interfaces* **2014**, *6*, 1835−1842.
(48) Yadav, S. K.; Mahapatra, S. S.; Cho, J. W.; Lee, J. Y. Functionalization of Multiwalled Carbon Nanotubes with Poly-(styrene-b-(ethylene-co-butylene)-b-styrene) by Click Coupling. *J. Phys. Chem. C* **2010**, *114*, 11395−11400.
(49) Lee, M.; Kim, J. U.; Lee, J. S.; Lee, B. I.; Shin, J.; Park, C. B. Mussel-Inspired Plasmonic Nanohybrids for Light Harvesting. *Adv. Mater.* **2014**, *26*, 4463−4468.
(50) Matyjaszewski, K.; Xia, J. Atom Transfer Radical Polymerization. *Chem. Rev.* **2001**, *101*, 2921−2990.
(51) Li, D.; Jang, Y. J.; Lee, J.; Lee, J.-E.; Kochuveedu, S. T.; Kim, D. H. Grafting Poly(4-vinylpyridine) onto Gold Nanorods toward Functional Plasmonic Core-Shell Nanostructures. *J. Mater. Chem.* **2011**, *21*, 16453−16460.
(52) Chen, H.; Zhang, Z.; Chen, Y.; Brook, M. A.; Sheardown, H. Protein Repellant Silicone Surfaces by Covalent Immobilization of Poly(ethylene oxide). *Biomaterials* **2005**, *26*, 2391−2399.
(53) Yu, Q.; Zhang, Y.; Wang, H.; Brash, J.; Chen, H. Anti-Fouling Bioactive Surfaces. *Acta Biomater.* **2011**, *7*, 1550−1557.
(54) Wu, J.; Mao, Z.; Gao, C. Controlling the Migration Behaviors of Vascular Smooth Muscle Cells by Methoxy Poly(ethylene glycol) Brushes of Different Molecular Weight and Density. *Biomaterials* **2012**, *33*, 810−820.
(55) Fan, X.; Lin, L.; Messersmith, P. B. Cell Fouling Resistance of Polymer Brushes Grafted from Ti Substrates by Surface-Initiated Polymerization: Effect of Ethylene Glycol Side Chain Length. *Biomacromolecules* **2006**, *7*, 2443−2448.
(56) Singh, N.; Cui, X.; Boland, T.; Husson, S. M. The Role of Independently Variable Grafting Density and Layer Thickness of Polymer Nanolayers on Peptide Adsorption and Cell Adhesion. *Biomaterials* **2007**, *28*, 763−771.
(57) Fristrup, C. J.; Jankova, K.; Eskimergen, R.; Bukrinsky, J. T.; Hvilsted, S. Protein Repellent Hydrophilic Grafts Prepared by Surface-Initiated Atom Transfer Radical Polymerization from Polypropylene. *Polym. Chem.* **2012**, *3*, 198−203.
(58) Chen, S.; Zheng, J.; Li, L.; Jiang, S. Strong Resistance of Phosphorylcholine Self-Assembled Monolayers to Protein Adsorption: Insights into Nonfouling Properties of Zwitterionic Materials. *J. Am. Chem. Soc.* **2005**, *127*, 14473−14478.
(59) Wu, J.; Chen, S. Investigation of the Hydration of Nonfouling Material Poly(ethylene glycol) by Low-Field Nuclear Magnetic Resonance. *Langmuir* **2012**, *28*, 2137−2144.
(60) Schaer, D. J.; Buehler, P. W.; Alayash, A. I.; Belcher, J. D.; Vercellotti, G. M. Hemolysis and Free Hemoglobin Revisited: Exploring Hemoglobin and Hemin Scavengers as a Novel Class of Therapeutic Proteins. *Blood* **2013**, *121*, 1276−1284.
(61) Kato, G. J.; Gladwin, M. T.; Steinberg, M. H. Deconstructing Sickle Cell Disease: Reappraisal of the Role of Hemolysis in the Development of Clinical Subphenotypes. *Blood Rev.* **2007**, *21*, 37−47.

(62) Gladwin, M. T.; Kanias, T.; Kim-Shapiro, D. B. Hemolysis and Cell-Free Hemoglobin Drive an Intrinsic Mechanism for Human Disease. *J. Clin. Invest.* **2012**, *122*, 1205−1208.
(63) Lee, S.-H.; Meng, X. W.; Flatten, K. S.; Loegering, D. A.; Kaufmann, S. H. Phosphatidylserine Exposure during Apoptosis Reflects Bidirectional Trafficking between Plasma Membrane and Cytoplasm. *Cell Death Differ.* **2012**, *20*, 64−76.
(64) Mariño, G.; Kroemer, G. Mechanisms of Apoptotic Phosphatidylserine Exposure. *Cell Res.* **2013**, *23*, 1247−1248.
(65) Wang, R.; Kreuzer, H.; Grunze, M. Molecular Conformation and Solvation of Oligo(ethylene glycol)-Terminated Self-Assembled Monolayers and Their Resistance to Protein Adsorption. *J. Phys. Chem. B* **1997**, *101*, 9767−9773.
(66) Vermes, I.; Haanen, C.; Steffens-Nakken, H.; Reutellingsperger, C. A Novel Assay for Apoptosis Flow Cytometric Detection of Phosphatidylserine Expression on Early Apoptotic Cells Using Fluorescein Labelled Annexin V. *J. Immunol. Methods* **1995**, *184*, 39−51.